

however, it does not involve an atypical enthalpy change, as compared with many reactions of current interest in both academic and industrial synthesis (Table 2). In general, analysis of combinatorial libraries should reveal novel catalyst structures with potentially new modes of catalysis, as observed here.

REFERENCES AND NOTES

1. F. M. Menger, A. V. Eliseev, V. A. Migulin, *J. Org. Chem.* **60**, 6666 (1995).
2. G. Liu and J. A. Ellman, *ibid.*, p. 7712; K. Burgess, H. J. Lim, A. M. Porte, G. Sulikowski, *Angew. Chem. Int. Ed. Engl.* **35**, 220 (1996); B. M. Cole *et al.*, *ibid.*, p. 1668.
3. K. S. Lam *et al.*, *Nature* **354**, 82 (1991); J. K. Chen, W. S. Lane, A. W. Brauer, A. Tanaka, S. L. Schreiber, *J. Am. Chem. Soc.* **115**, 12591 (1993); A. Borchardt and W. C. Still, *ibid.* **116**, 373 (1994); M. T. Burger and W. C. Still, *J. Org. Chem.* **60**, 7382 (1995); M. B. Francis, N. S. Finney, E. N. Jacobsen, *J. Am. Chem. Soc.* **118**, 8983 (1996); H. P. Nestler, H. Wenemers, R. Sherlock, D. L. Y. Dong, *Bioorg. Med. Chem. Lett.* **6**, 1327 (1996).
4. I. P. Nagy and J. A. Pojman, *Chem. Phys. Lett.* **200**, 147 (1992); K. Kustin and E. W. Ross, *J. Chem. Educ.* **70**, 454 (1993); I. Eskendirov, B. Kabongo, L. Glasser, V. D. Sokolovskii, *J. Chem. Soc. Faraday Trans.* **91**, 991 (1995).
5. F. C. Moates *et al.*, *Ind. Eng. Chem. Res.* **35**, 4801 (1996).
6. E. Vedejs and X. Chen, *J. Am. Chem. Soc.* **118**, 1809 (1996); J. C. Ruble and G. C. Fu, *J. Org. Chem.* **61**, 7230 (1996); J. C. Ruble, H. A. Latham, G. C. Fu, *J. Am. Chem. Soc.* **119**, 1492 (1997); T. Kawabata, M. Nagato, K. Takasu, K. Fuji, *ibid.*, p. 3169.
7. A. Fersht and W. P. Jencks, *J. Am. Chem. Soc.* **92**, 5432 (1970); E. Guibe-Jampel, G. Le Corre, M. Wakselman, *Tetrahedron Lett.* 1157 (1979); G. Hofle, W. Steglich, H. Vorbruggen, *Angew. Chem. Int. Ed. Engl.* **17**, 596 (1978); E. Vedejs and S. T. Diver, *J. Am. Chem. Soc.* **115**, 3358 (1993).
8. For relevant studies, see E. J. Delaney, L. E. Wood, I. M. Klotz, *J. Am. Chem. Soc.* **104**, 799 (1982); M. Tomoi, Y. Akada, H. Kakiuchi, *Makromol. Chem. Rapid Commun.* **3**, 537 (1982); F. M. Menger and D. J. McCann, *J. Org. Chem.* **50**, 3928 (1985); A. Deratani, G. D. Darling, D. Horak, J. M. J. Fréchet, *Macromolecules* **20**, 767 (1987).
9. M. H. Ohlmeyer *et al.*, *Proc. Natl. Acad. Sci. U.S.A.* **90**, 10922 (1993).
10. A. Furka, F. Sebestyén, M. Asgedom, G. Dibo, *Int. J. Pept. Protein Res.* **37**, 487 (1991).
11. Library synthesis was performed on aminomethyl polystyrene macrobeads (500 μm , 1.04 mmol/g; Rapp Polymere, Tübingen, Germany), because catalysts on this polymer support were found to give a larger temperature increase in a related assay developed in our labs.
12. A. P. Combs *et al.*, *J. Am. Chem. Soc.* **118**, 287 (1996).
13. **B12** was prepared by treatment of L-proline *tert*-butyl ester (2 equiv.) and 4-bromopyridine (1 equiv.) with diisopropylethylamine (3 equiv) in dimethyl sulfoxide at 120°C for 12 hours.
14. Synthesis efficiency or site-site interactions between multiple catalyst moieties may lead to variation in observed activity that does not reflect inherent activity. In regard to catalyst synthesis, preliminary data indicate that the syntheses were successful in the preparation of **1**, **2**, and **5**. Catalyst resynthesis on Rink amide resin (Novabiochem) followed by cleavage from solid support afforded a compound with very clean low-resolution fast atom bombardment mass spectra corresponding to the predicted product in each case. Although these results are not quantitative and are somewhat ambiguous because a different resin was used in resynthesis as compared with library preparation, they do indicate that no fundamental synthesis problems occurred during

the preparation of these monomer sequences.

15. J. D. Cox and G. Pilcher, *Thermochemistry of Organic and Organometallic Compounds* (Academic Press, New York, 1970).
16. We thank L. H. Bogart of Cincinnati Electronics (Ma-

son, OH) and R. E. Richardson of Mec-Tric Control (Charlotte, NC) for assistance and use of the Cincinnati Electronics IRRIS-256ST IR camera.

6 October 1997; accepted 23 February 1998

Polyolefin Spheres from Metallocenes Supported on Noninteracting Polystyrene

Stephen B. Roscoe, Jean M. J. Fréchet,* John F. Walzer, Anthony J. Dias

To obviate the destructive interaction of highly reactive metallocene catalysts with classical silica-based supports while retaining the advantage of supported catalysts, a noninteracting polystyrene support was developed. Supported catalysts for the polymerization of α -olefins are prepared by treating lightly cross-linked, chloromethylated polystyrene beads consecutively with a secondary amine, an ammonium salt of a weakly coordinating anion, and a neutral dialkylmetallocene. Catalytic sites are distributed homogeneously throughout the support particle, and the polymerization occurs within the bead, in contrast to traditional surface-supported metallocene catalysts. The copolymerization of ethylene and 1-hexene at 40°C affords discrete spherical polyolefin beads with a size (0.3 to 1.4 millimeters) that varies according to the polymerization time.

The polymerization of α -olefins by metallocene-based catalysts is at an exciting juncture. Research into a wide variety of cationic metallocene structures, and attendant weakly coordinating anions, has led to the development of families of highly active and selective catalysts, which generate a range of polyolefin products in solution (1). However, practical considerations have dictated that industrial olefin polymerizations be performed usually in the heterogeneous mode with supported catalysts. Traditional supports, such as high surface area silica or alumina, have received the most attention and indeed have proven immensely successful in the commercial-scale production of polyolefins. Such acidic supports, however, have reactive surfaces that can lead to catalyst deactivation and thus alternate supports are desirable. We have focused our attention on silica-free supports designed for chemical versatility and rugged physical properties to best exploit state-of-the-art catalysts (2). Our approach to designing the support material aims at functionalizing the interior of a swellable but insoluble polymer particle with the appropriate catalyst to allow a nominally heterogeneous polymerization to proceed in a microscopically homogeneous "solution-like" environment. The use of an organic substrate allows us to select a sequence of facile, high-yielding reactions for catalyst preparation (making the procedure well suited for practical uses) or for the combinatorial

investigation of α -olefin polymerization. We report here a modular polystyrene (PS)-based support technology that not only yields supported catalysts unusually active at low temperatures but also generates polyethylene-co-hexene in the form of discrete, free-flowing, millimeter-sized spheres that grow in proportion to the polymerization time.

The functionalization of polymer resin beads provides an especially suitable method to tailor a heterogeneous catalytic moiety in much the same manner as a homogeneous catalyst. Lessons learned in solution about the design of a catalytic complex may be applied more reliably to a polymer matrix than to the surface of an inorganic support, because an organic material can be designed to more closely resemble the solution environment (3). Numerous routes are available for the functionalization of solid resin beads, and a number of polymer-bound catalytic systems have been devised for several important reactions (4), including olefin metathesis (5) and Ziegler-Natta polymerizations (6, 7). Many of these systems exhibit not only different kinetics, but also different regio- (8) and enantio-selectivities (9) from their homogeneous and heterogeneous counterparts.

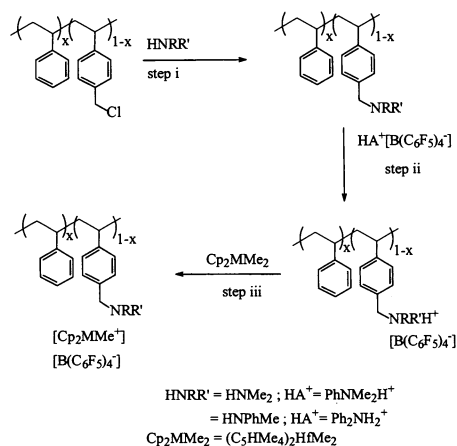
The group IV metallocene catalysts are generated from a neutral precursor complex that is activated by a cocatalyst, such as the combination of a Lewis or Brønsted acid, to abstract a ligand from the metallocene generating a low-valent cation, and a charge-balancing noncoordinating counterion. In many systems described previously, an oligomeric product from the partial hydrolysis of trimethylaluminum (methylalu-

S. B. Roscoe and J. M. J. Fréchet, Department of Chemistry, University of California, Berkeley, CA 94720, USA. J. F. Walzer and A. J. Dias, Baytown Polymer Center, Exxon Chemical Company, 5200 Bayway Drive, Baytown, TX 77520, USA.

moxane or MAO) (10) was used to fulfill the functions of both acid and counterion, although better characterized cocatalysts, such as the trityl (11) or trialkylammonium (12) salts of tetrakis(pentafluorophenyl)borate $[R_3NH][B(C_6F_5)_4]$, have also been exploited. Although there is considerable work on the development of heterogeneous catalysts based on metallocenes, their extreme sensitivity to polar impurities makes standard inorganic supports such as silica less than ideal in all but larger scale industrial applications.

Recent work on supporting group IV metallocenes on inert organic substrates for olefin polymerization (7) focused on designing a polymer-supported ligand with which to bind the reactive metal center. We selected an alternative strategy of functionalizing the support with the other components used to generate the active catalyst. A lightly cross-linked, swelling polymer disperses catalytically active molecules homogeneously throughout the particle, rather than localizing them on the surface, as in traditional supported catalysts. Thus, swellable PS beads, cross-linked with 1% divinylbenzene, provide an isotropic, dynamic, hydrocarbon-based microenvironment. This support provides a much closer analog to the environment experienced by soluble metallocene catalysts and is in sharp contrast to the rigid, anisotropic inorganic surfaces commonly exploited for supported catalysts.

Stirring commercially available chloromethylated polystyrene-co-divinylbenzene beads with an excess of dimethylamine yields the basic tertiary amine functionalized polymer (Scheme 1) (13). Treatment



Scheme 1. Sequential functionalization of chloromethylated polystyrene-co-divinylbenzene beads with (i) a secondary amine, (ii) an acidic salt of the tetrakis(perfluorophenyl)boron anion, and (iii) a dimethylmetallocene.

of the polymer-bound amine with a standard activator salt, $[PhNMe_2H][B(C_6F_5)_4]$ (Ph, phenyl, Me, methyl), protonates the basic resin and binds the perfluorinated borate anion to the support by ion pairing.

Table 1. Polymerization data for five representative catalysts at 40°C. GPC, gel permeation chromatography; MWD, molecular weight distribution; meq, millimoles of catalyst per gram.

Catalyst bead (mg)	Loading (meq)	Run time (min)	Yield (g)	Bulk prod.*	Specific activity† ($\times 10^5$)	GPC (M_w)	MWD	Hexene (weight %)
A (60)	0.52	30	33.5	219	4.22	99,600	2.9	21.3
B (100)	0.52	30	36.2	142	2.74	94,600	2.8	18.7
C (150)	0.24	30	55.5	145	6.06	178,700	3.6	21.7
D (100)	0.52	60	51.1	100	1.93	147,700	4.3	16.1
E (72)	0.24	120	111.7	152	6.29	188,700	7.3	14.8

*Assessed as grams of polymer per gram of catalyst per atmosphere per hour.

†Assessed as grams of polymer per mole of metallocene per atmosphere per hour.

The readily soluble $PhNMe_2$ by-product can be washed out with organic solvents, thus effectively transferring $HB(C_6F_5)_4$ to the solid support without generating any solid by-products. The active catalyst is then generated, at loadings varying from 0.14 to 0.77 milliequivalents of metallocene per gram, by treating the borated beads with a toluene solution of a metallocene such as bis(tetramethylcyclopentadienyl) dimethylhafnium.

Each of the three steps proceeds in high yield and can be driven essentially to completion by the use of an excess of reagent, and the by-products are easily removed from the support. Furthermore, each of the three components can be easily and independently varied by use of the appropriate reagent. The only requirements are that the amine component must be sufficiently nucleophilic to displace a benzylic halide (Scheme 1, step i), the ammonium salt must be more acidic than the polymer-bound amine (step ii), and the metallocene must be capable of reacting with a tertiary ammonium cation to generate a free amine, methane, and a metallocenium cation (step iii).

The supported catalysts display excellent activity for the slurry-phase copolymerization (14) of ethylene and 1-hexene (Table 1). At 40°C, typical activities are in the range of 2×10^5 to 4×10^5 grams of polymer per mole of metallocene per atmosphere per hour (Table 1). Significantly, the product is isolated in the form of discrete spherical beads of millimeter dimension, with a distribution of sizes similar to that of the starting PS beads (Fig. 1, A and B). This finding implies that each polymer particle results from the polymerization of an individual catalytic bead. The size of the product beads depends on the reaction time; beads produced by longer reaction times (up to 2 hours) exhibited correspondingly greater radii, and the catalyst still retained its activity after this time. The particle size distribution of the polyolefin beads obtained after 30 min of polymerization at 40°C is shown in Fig. 1C. Gel permeation chromatography analysis of the product polymer revealed weight-average molecular weights (M_w) in the range

of 80,000 to 180,000, with typical polydispersities of 3 to 4. These weights are in the typical range for metallocene catalysts, and although the polydispersities are higher than

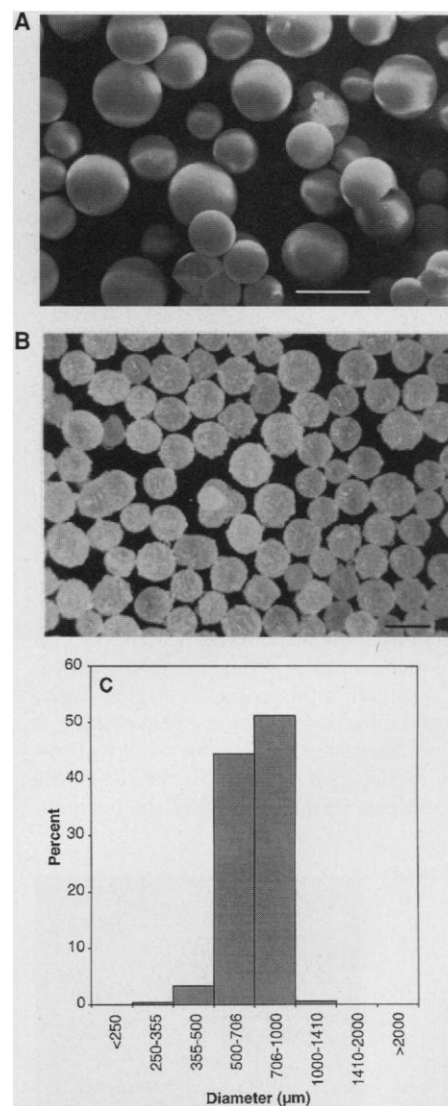


Fig. 1. (A) Scanning electron microscope image of a metallated catalyst particle (scale bar, 100 μ m). (B) Optical microscope image of a product bead (scale bar, 1 mm). (C) Particle size distribution for the polyolefin beads obtained after 30 min of polymerization at 40°C.

ideal, this may be attributed in part to the high hexene consumption. This is particularly significant in the 2-hour polymerization (Table 1), where more than 50% of the available hexene was consumed during the course of the reaction.

The generation of homogeneously polymerized polyethylene by active cation-anion pairs leached out of the beads would clearly be a concern because it is implicit in this strategy that neither cation nor anion are actually bound to the support. However, the presence of the Lewis basic amine and the higher polarity of the PS matrix relative to the hexane-hexene liquid phase preclude extraction of the catalyst. The activated beads are further washed with toluene to remove any extractable catalyst or unreacted, neutral metallocene before the polymerization. Time of flight secondary ion mass spectrometry (TOF-SIMS) mapping of the boron concentration (15) in a cross section of a catalyst bead (Fig. 2) demonstrates that the borate anions, and thus the metallocene cations, are homogeneously distributed throughout the particle. This result provides further evidence that the polymerization is occurring within the PS particle rather than on a thin surface layer, as is the case for traditional supported catalysts. The effect of diffusion into the lightly cross-linked PS catalyst beads should therefore be considered when assessing the catalyst activity.

The ethylene uptake curve for a typical 1-hour polymerization (Fig. 3) indicates that there is only a slight loss in activity during the course of the reaction. The ethylene consumption rate after 1 hour is ~60% of its maximum value, which is achieved after 30 min. This result attests to the prolonged active life of the catalyst bead, but it is uncertain whether this is related to the life span of individual catalytically active species or to increased access to new catalytic sites as the polymerization progresses. Figure 3 also reveals an induction time at the beginning of the polymerization, which we tentatively assign to slow swelling of the beads in the hexane-hexene mixture. Thus, the polymer-

ization rate is low, perhaps confined to the outer layers of the bead, until the bead swells sufficiently to allow permeation of the monomers into the interior sites. The polymerization then enters a diffusion-controlled regime, with the rate increasing as the polymer bead swells, until a maximum rate is reached after about 30 min. The gradual reduction in rate for the rest of the reaction may be attributed to several different causes, including slow consumption of active metallocenes or reduced permeability of the product polymer as the reaction proceeds. This reduced permeability is a function of the limited hexene supply, a considerable proportion of which is consumed during the course of polymerization. As the polymerization progresses, this leads to a lower incorporation of hexene and a higher degree of crystallinity of the product polymer.

Despite the high levels of hexene incorporation (15 to 30% by weight), the product polymer is isolated as discrete, free-flowing beads. The large size and spherical morphology of these beads, for which the polymer-supported catalyst acts as a shape template, is of particular commercial relevance. A regular spherical shape is the ideal result in industrial-scale polymerizations, where particles of very small or highly variable sizes or those that have grossly irregular shapes interfere with the efficiency and general operation of the reactor.

Increasing the polymerization temperature from 40° to 60°C leads to a high reaction rate accompanied by a considerable exotherm that prevents kinetic analysis. However, the morphology of the resulting polymer is poor, with particles of very small and variable and ill-defined shapes. These particles are generally much smaller than the starting beads, suggesting that rapid and uncontrolled destruction of the active catalyst particles occurs. We anticipate that a lower loading of active metallocene should allow the use of higher reaction temperatures while avoiding unacceptable exothermicity.

As a demonstration of the generality of the technique and its applicability to combinatorial techniques, catalysts were also prepared with *N*-methylaniline, yield-

ing a polymer-bound benzylmethylaniline that could be protonated with $[\text{Ph}_2\text{NH}_2][\text{B}(\text{C}_6\text{F}_5)_4]$ (Scheme 1). These samples were treated with the same metallocene to yield active polymerization catalysts.

An appealing feature of this polymer-supported catalyst is its versatility. Functional versatility is expressed in the ability to obtain directly millimeter-size spheres of the desired polyolefin, whereas the ability to vary independently each of the three components of the catalyst affords an easy route to the comparative testing of various metallocenes. This approach allows for the ready variation of the metallocene component simply by treating the beads with the appropriate metallocene precursor. Therefore, this synthetic strategy could provide the basis for the rapid screening of metallocene catalyst systems, prepared in parallel or through combinatorial chemistry (16). One support might be used with a whole library of metallocene complexes, allowing direct comparison of ligand effects in a heterogeneous system.

REFERENCES AND NOTES

1. M. Bochmann, *J. Chem. Soc. Dalton Trans.* **1996**, 255 (1996); H.-H. Brintzinger, D. Fischer, R. Mülhaupt, B. Rieger, R. M. Waymouth, *Angew. Chem. Int. Ed. Engl.* **34**, 1143 (1995); P. C. Möhring and N. J. Coville, *J. Organomet. Chem.* **479**, 1 (1994); T. J. Marks, *Acc. Chem. Res.* **25**, 57 (1992).
2. See, for example, G. W. Coates and R. M. Waymouth, *Science* **267**, 217 (1995); L. K. Johnson, S. Mecking, M. Brookhart, *J. Am. Chem. Soc.* **118**, 267 (1996); L. K. Johnson, C. M. Killian, M. Brookhart, *ibid.* **117**, 6414 (1995).
3. R. H. Grubbs, *Chemtech* **7**, 512 (1977).
4. J. M. J. Fréchet and M. J. Farrell, in *Chemistry and Properties of Crosslinked Polymers*, S. S. Labana, Ed. (Academic Press, New York, 1977), pp. 59–83.
5. S. T. Nguyen and R. H. Grubbs, *J. Organomet. Chem.* **497**, 195 (1995).
6. L. Sun, A. Shariati, J. C. Hsu, D. W. Bacon, *Stud. Surf. Sci. Catal.* **89**, 81 (1994); L. Sun, C. C. Hsu, D. W. Bacon, *J. Polym. Sci. Part A* **32**, 2127 (1994); S. A. Mkrtchyan *et al.*, *Polym. Sci. USSR* **28**, 2343 (1986).
7. K. Soga, T. Arai, B. T. Hoang, T. Uozumi, *Macromol. Rapid Commun.* **16**, 905, (1995); H. Nishida, T. Uozumi, T. Arai, K. Soga, *ibid.*, p. 821.
8. R. H. Grubbs, E. M. Sweet, S. Phisanbut, in *Catalysis in Organic Synthesis*, P. Rylander and H. Greenfield, Eds. (Academic Press, New York, 1976), pp. 153–160; B. M. Trost and E. Kienan, *J. Am. Chem. Soc.* **100**, 7780 (1978); J. F. McQuillin, W. O. Ord, P. L. Simpson, *ibid.* **1963**, 5996 (1963).
9. S. Itsuno *et al.*, *J. Org. Chem.* **55**, 304 (1990); S. Itsuno and J. M. J. Fréchet, *ibid.* **52**, 4140 (1987).
10. W. Kaminsky, *Catal. Today* **20**, 257 (1995).
11. J. C. W. Chien, W.-M. Tsai, M. D. Rausch, *J. Am. Chem. Soc.* **113**, 8570 (1991).
12. X. Yang, C. Stern, T. J. Marks, *Organometallics* **10**, 840 (1991); G. G. Hlatky, D. T. Upton, H. W. Turner, U.S. Patent Application 459921 (1990).
13. K. W. Pepper, H. M. Paisley, M. A. Young, *J. Chem. Soc.* **1953**, 4097 (1953).
14. Table 1 shows data for two representative bead loadings of 0.52 and 0.24 mmol of $(\text{C}_5\text{HMe}_4)_2\text{HfMe}_2$ catalyst per gram. The dimethylamine-modified beads were prepared from 1% cross-linked PS containing 1.25 and 0.4 milliequivalents of chlorometal pendant groups per gram, respectively. The ethylene pressure was 75 psi; the reactor contained 45 ml of hexene and 400 ml of hexane.

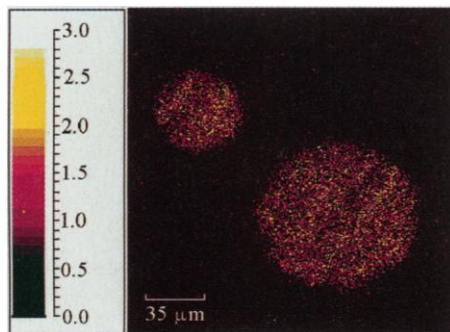


Fig. 2. TOF-SIMS map (^{11}B) of the cross section of two PS catalyst beads.

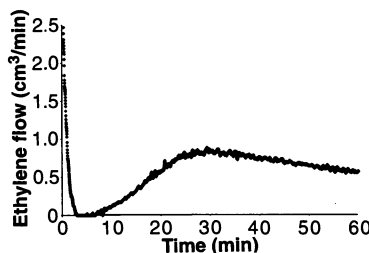


Fig. 3. Ethylene consumption versus polymerization time for a representative 1-hour polymerization run.

15. The low mass of the ^{11}B nucleus makes it the optimal ion for detection of cation-anion pairs in the catalyst bead. A sample of catalyst was mounted in a resin matrix and then microtomed to give a flat surface for the SIMS analysis. Figure 3 shows two beads, one of which displays a larger cross section than the other

- because it was machined to a different depth.
 16. X.-D. Xiang *et al.*, *Science* **268**, 1738 (1995).
 17. This work partially funded from NSF grant DMR-9641291 to J.F.

28 October 1997; accepted 20 February 1998

Friction Anisotropy and Asymmetry of a Compliant Monolayer Induced by a Small Molecular Tilt

M. Liley,* D. Gourdon, D. Stamou, U. Meseth, T. M. Fischer, C. Lautz, H. Stahlberg,† H. Vogel, N. A. Burnham, C. Duschl‡

Lateral force microscopy in the wearless regime was used to study the friction behavior of a lipid monolayer on mica. In the monolayer, condensed domains with long-range orientational order of the lipid molecules were present. The domains revealed unexpectedly strong friction anisotropies and non-negligible friction asymmetries. The angular dependency of these effects correlated well with the tilt direction of the alkyl chains of the monolayer, as determined by electron diffraction and Brewster angle microscopy. The molecular tilt causing these frictional effects was less than 15 degrees, demonstrating that even small molecular tilts can make a major contribution to friction.

Although the nature of friction has been debated since da Vinci's time, a fundamental understanding of friction phenomena has remained elusive. Amontons formulated his law relating friction and the normal load 300 years ago; a hundred years later, Coulomb interpreted friction in terms of cobblestones in a rough road—the bigger the stones, the higher the friction (1). In this century, friction has come to be construed as the plastic degradation of interlocking asperities (2), or to be related to adhesion hysteresis (3). The effect of crystallographic direction on friction was first demonstrated on mica with the surface forces apparatus (4) and later on an organic bilayer with lateral force microscopy (LFM) (5). Recent results, obtained exclusively by LFM, indicated that molecular orientation may also influence friction (6, 7), but no independent structural data were available. Here, we correlated friction data with the molecular orientation as established

by independent methods.

A monolayer of a chiral lipid (8) at the air-water interface was compressed to the coexistence regime where condensed domains form in a fluid matrix (9). This monolayer was transferred to a mica substrate so that the lipids were oriented with the polar head groups toward the mica surface and the alkyl chains exposed to the air (10). LFM (11) on the monolayer revealed flower-like condensed domains. In the lateral force images of the domains (Fig. 1, A and B), each petal of the flower has a different amount of lateral force, whereas the corresponding topography images (not shown here) display no contrast between the different petals (12). For flat samples such as these, the lateral force is equivalent to the tip-sample friction. In the domain shown, there are six major petals and two minor petals. The major petals all have equivalent molecular organization. The minor petals are the result of rotational twinning; they have the same molecular organization as the adjacent major petal, but rotated through 180° (13).

Upon rotation of the sample underneath the microscope tip (Fig. 1B), the friction force on the petals changes in a systematic way. These changes were analyzed using "friction loops" (Fig. 1C), where each loop corresponds to one scan line of the image. The friction force amplitudes L and R for the two scan directions yield the "total friction" $L + R$ and the "friction asymmetry" $L - R$ (14). The variations of the amplitudes L and R correspond to $\sim 25\%$ of the overall friction force.

The total friction and the friction asymmetry were analyzed as a function of the subdomain's angular orientation θ with respect to the scan direction (Fig. 1A); the results of this analysis are shown in Fig. 1, D and E. For both the major and minor subdomains, the total friction has C_2 symmetry (180° periodicity) and the friction asymmetry has C_1 symmetry (360° periodicity). In other words, the friction is not only anisotropic—dependent on the angle of the tip's motion with respect to the domain orientation—but is also asymmetric, that is, different for the trace and retrace of the force microscope tip over the same scan line. There are also differences between the major petals (filled circles) and minor petals (open circles). The two total friction curves are displaced by 30° , a difference that is caused entirely by our definition of the angular direction of the petals. The two friction asymmetry curves are offset by 150° to 210° , which confirms the 180° rotation of molecular organization between major and minor arms.

As a refinement of our analysis, we used the fits of the total friction ($L + R$) and friction asymmetry ($L - R$) to produce simulated lateral force data and images, which we compared with the experimental images. Total friction minus friction asymmetry gave the friction values, R , for the right-to-left scans as a function of angle. These friction values defined the gray levels for the different petals in the simulated images. The success of this simulation of the experimental data (compare Figs. 1B and 1F) allowed us to fix with some certainty the phase angles and relative magnitudes of the fit curves. We conclude that maximum total friction and zero friction asymmetry occurred at 30° , and that the two effects had an amplitude ratio of 10:1.

These friction results led us to investigate the structure of the lipid monolayers. Electron diffraction (Fig. 2A) revealed a hexagonal packing of the alkyl chains (15), with the nearest neighbor directions approximately parallel to the edges of the domain boundaries. The tilt angle of the alkyl chains (to the normal) was estimated to be less than 15° from the normal.

We used Brewster angle microscopy (16) to obtain essential information about the tilt angle of the alkyl chains and their tilt direction (azimuthal angle); this technique is based on the reflection of p-polarized light and allows local determination of these parameters. Experimental images were compared with images (Fig. 2B) calculated using well-established parameters for lipid monolayers (17). The best agreement was obtained for a tilt angle of the alkyl chains of $10^\circ \pm 5^\circ$. The tilt direction was found to lie parallel to the subdomain boundary, as indi-

M. Liley, D. Stamou, U. Meseth, H. Vogel, C. Duschl, Department of Chemistry, Swiss Federal Institute of Technology, CH-1015 Lausanne, Switzerland.

D. Gourdon and N. A. Burnham, Department of Physics, Swiss Federal Institute of Technology, CH-1015 Lausanne, Switzerland.

T. M. Fischer and C. Lautz, Department of Physics, University of Leipzig, Linnéstraße 5, D-04103 Leipzig, Germany.

H. Stahlberg, Department of Chemistry, Swiss Federal Institute of Technology, CH-1015 Lausanne, Switzerland, and Department of Biology, University of Lausanne, CH-1015 Lausanne, Switzerland.

*Present address: Centre Suisse d'Electronique et Microtechnique SA, CH-2007 Neuchâtel, Switzerland.

†Present address: Biocenter, University of Basel, CH-4056 Basel, Switzerland.

‡To whom correspondence should be addressed. E-mail: duschl@igcsun3.epfl.ch